Journal of Power Sources 201 (2012) 402–407

Contents lists available at SciVerse ScienceDirect

Journal of Power Sources

journal homepage: www.elsevier.com/locate/jpowsour

Short communication

A low cost mesoporous carbon/SnO_2/TiO_2 nanocomposite counter electrode for dye-sensitized solar cells

Weiwei Sun [a], Xiaohua Sun [a], Tao Peng [a], Yumin Liu [a], Hongwei Zhu [a], Shishang Guo [a,b], Xing-zhong Zhao [a,b,*]

[a] School of Physics and Technology, Wuhan University, Wuhan 430072, People's Republic of China
[b] Key Laboratory of Artificial Micro/Nano Structures of Ministry of Education, Wuhan University, Wuhan 430072, People's Republic of China

ARTICLE INFO

Article history:
Received 2 June 2011
Received in revised form 28 October 2011
Accepted 30 October 2011
Available online 4 November 2011

Keywords:
Porous
Tin oxide
Nanocomposite
Framework
Dye-sensitized solar cells

ABSTRACT

Highly porous carbon/SnO_2/TiO_2 nanocomposite films that can be used as counter electrodes in dye-sensitized solar cells (DSSCs) are fabricated by coating a homogeneous and viscous carbon paste on F-doped tin oxide conducting glass. The carbon paste is prepared by ball-milling a mixture of carbon, SnO_2 powder and TiO_2 hydrosol in an organic solution. The composite films are characterized by X-ray diffraction, scanning electron microscopy, transmission electron microscope, Brunauer–Emmett–Teller and Form Talysruf Profiler. The results indicate that the photovoltaic performances of the composite DSSCs are influenced by the content of SnO_2. When the content is increased to 30%, SnO_2 not only acts as "framework" to strengthen the mechanical stability of the composite film but also increases the specific surface area and root-mean-square roughness, which improve fill factor and short-circuit current, finally increasing power conversion efficiency from 5.12% to 6.15%. Cyclic voltammetry analysis and electronic impedance spectroscopy of the optimum composite film display higher catalytic activity for I_3^-/I^- redox reactions and much lower charge-transfer resistance compared with Pt, respectively. Dye-sensitized solar cells based on this nanocomposite counter electrode achieve efficiency as high as 6.15% which is comparable to that of the cells using sputtering Pt as counter electrode at similar conditions.

1. Introduction

Since initially reported by O'Regan and Grätzel in 1991, dye-sensitized solar cells (DSSCs) have been considered as a credible alternative to the conventional silicon solar cells for their easy fabrication, low cost and high-energy conversion efficiency [1,2]. Typically, standard DSSCs consist of a dye-sensitized mesoporous semiconductor photoanode, an iodide/tri-iodide redox electrolyte, and a catalytic counter electrode. The counter electrode is an important component of the DSSCs, the roles of which are to collect electrons from external circuit and reduce I_3^- to I^- in electrolyte. Usually fluorine-doped tin oxide (FTO) glass is loaded with platinum to facilitate electron transfer from external circuit to I_3^-/I^- redox electrolyte, duo to the high catalytic activity and conductivity of platinum [3,4]. However, platinum is a noble metal and both of the two current methods, sputtering and electrochemical deposition [5,6], used for preparing Pt counter electrodes are high energy-consuming, which would limit the industrial applications. Therefore, many studies have been devoted to finding new alternative materials with low cost, high electronic conductivity, good chemical stability, and comparable catalytic effects for tri-iodide reduction to replace platinum as counter electrodes for DSSCs. And carbon is a promising candidate.

Recently some emphases have been focused on carbonaceous materials including carbon, graphite, hard carbon sphere, carbon nanotubes and graphene due to their wonderful conductivity and extremely low cost [7–10]. Unfortunately, nano-size carbon counter electrode posed an additional risk to the stability of DSSCs for prolonging exposure in corrosive I_3^-/I^- redox electrolyte, which may lead to the detachment of loosely bounded particles from rest of the electrode [11]. For this reason, to form a high quality carbon film on the substrate as the counter electrode was crucial. Several methods have been reported to solve this problem [12,13]. The carbon/TiO_2 composite prepared by spin-coating method has been served as a counter electrode catalyst for tri-iodide reduction, where carbon acts as a catalyst and the TiO_2 functions as a binder. To a certain extent, the composite counter electrode enhanced the stability of the cell and achieved good conversion efficiency for DSSCs [13]. Meanwhile, some studies were reported that SnO_2 can connect with carbon surfaces to strengthen the mechanical stability of the carbon film [14,15], which made it possible to increase the photovoltaic performances of carbon based DSSCs.

* Corresponding author at: School of Physics and Technology, Wuhan University, Wuhan 430072, People's Republic of China. Tel.: +86 27 87642784; fax: +86 27 87642569.
E-mail address: xzzhao@whu.edu.cn (X.-z. Zhao).

0378-7753/$ – see front matter © 2011 Elsevier B.V. All rights reserved.
doi:10.1016/j.jpowsour.2011.10.097

In this paper, we prepared carbon/SnO_2/TiO_2 nanocomposite counter electrode by coating a homogeneous and viscous carbon paste on FTO substrate. In the carbon/SnO_2/TiO_2 nano-composite, carbon black and graphite were employed as catalyst to reduce I_3^-, the SnO_2 acted as the "framework" of the carbon film while the TiO_2 functioned as a binder. As a result, this nanocomposite counter electrode showed a good stability to prolong the corrosion of the electrolyte, and obtained remarkable conversion efficiency. DSSCs based on this nanocomposite counter electrode proved a comparable performance to Pt counter electrode based devices at similar conditions.

2. Experimental

2.1. Materials and reagents

Carbon black powder (particle size: 50 nm), graphite powder (particle size: 10 μm), SnO_2 powder (particle size: 10–500 nm), Poly (ethylene glycol) (PEG, MW = 20,000), Triton-X100, ethylene glycol, hydrogen nitrate (HNO_3), citric acid, acetic acid (CH_3COOH), and acetylacetone were obtained from Sinopharm Chemical Reagent Corporation (China). Lithium iodide (LiI, 99%), 4-tert-butylpyridine (TBP) and titanium tetraisopropoxide (98%) were purchased from Acros. Iodine (I_2, 99.8%) was obtained from Beijing Yili chemicals (China). The Ru dye, *cis*-di(thiocyanato)-bis(2,2′-bipyridyl-4,4′-dicarboxylate) ruthenium(II) (N719), were purchased from Solaronix (Switzerland). All the reagents used were of analytical purity. Fluorine-doped SnO_2 conductive glass (FTO, square resistance 10–15 Ω sq^{-1}, Asahi Glass, Japan) were used as the substrate for doctor-bladed the carbon/SnO_2/TiO_2 nanocomposite electrode and the deposition of mesoporous nanocrystalline TiO_2 film.

2.2. Preparation of carbon and Pt counter electrodes

The carbon paste was prepared as follows: 2 g of graphite, 1 g of carbon black and SnO_2 powder with various weights were dispersed in 15 g of ethanediol. Then the mixture was ball-milled at 300 r min^{-1} for 3 h. After that, 12 g of citric acid was added into the mixture. By means of one night ball-milling, the carbon suspension was turned to a homogeneous and viscous paste. Finally, 3 ml of TiO_2 hydrosol was dropt to carbon paste for 3 h's ball-milling. The TiO_2 hydrosol was synthesized by hydrolysis of titanium tetraisopropoxide according to the reported procedure [16]. In short, titanium tetraisopropoxide was added into glacial acetic acid under stirring for 10 min, and the mixture was then injected into HNO_3 aqueous solution under stirring and heating at 80 °C for 8 h. The carbon/SnO_2/TiO_2 nanocomposite electrode was prepared by coating the viscous paste on FTO conductive glass sheet using doctor-bladed method and then sintered at 450 °C for one night. Meanwhile, the Pt electrode was prepared by depositing a thin layer of Pt on FTO using magnetron sputtering.

2.3. Preparation of DSSCs

TiO_2 paste synthesized by hydrothermal method was doctor-bladed on FTO glass and sintered at 500 °C for 30 min. Subsequently, the TiO_2 photoanode was immersed in a 0.5 mM N3 ethanol solution and heated at 60 °C for 12 h, then rinsed with ethanol and dried. A liquid electrolyte was prepared by blending 1 M PMII(1-methyl-3-propyl imidazolium iodide), 0.04 M LiI, 0.03 M I_2, 0.1 M GuSCN(guanidinium thiocyanate), 0.5 M TBP(4-tert-butylpyridine) in acetonitrile, and propylene carbonate(v/v = 1:1) between them. The sandwich-type DSSCs were assembled by dropping a drop of the liquid electrolytes on the dye-sensitized TiO_2 film and then Pt or carbon counter electrode was clipped firmly with the TiO_2 photoanode. A mask with a window of 0.25 cm^2 was also clipped on the TiO_2 side to define the active area of the cell.

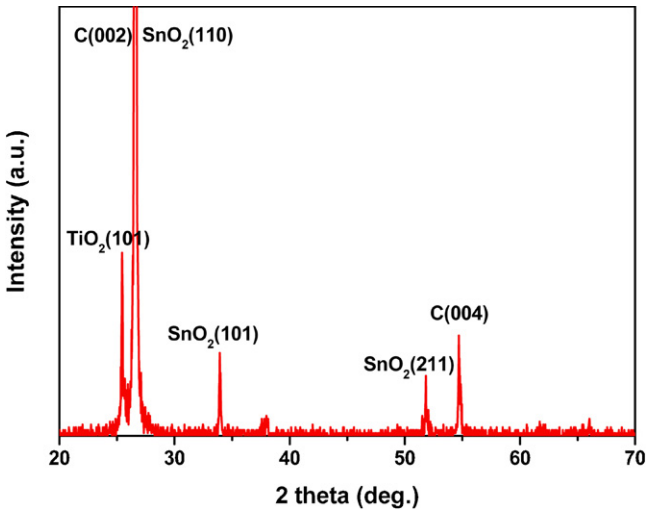

Fig. 1. X-ray diffraction pattern of the carbon powder scraped from the carbon film.

2.4. Characterization

The specific surface area and roughness of the carbon film were investigated by Brunauer–Emmett–Teller (BET) nitrogen sorption–desorption measurement (JW-BK, China) [17] and Form Talysruf Profiler (S4C-3D, England), respectively. The crystal structure of the carbon film was measured by XRD (D8 Advance, Bruker, Germany) using Cu Kα radiation. Scanning electron microscopy, SEM (JEOL, 6700F, Japan) was applied to study the morphology and microstructure of the carbon film. TEM and HRTEM investigations were carried out using a JEOL2010, equipped with an energy dispersive X-ray analysis (EDX) system. Cyclic voltammetry was performed on CHI 660C (Shang Hai, China) electrochemical station with a Pt as auxiliary electrode, a Hg/Hg^+ electrode as reference electrode, and Pt/FTO or carbon/FTO as working electrode in an acetonitrile solution containing 10 mM LiI, 1 mM I_2, and 0.1 M $LiClO_4$ as supporting electrolyte at a scan rate of 50 mV s^{-1}. The current–voltage characteristics of the cells were recorded by applying external potential bias to the device under AM1.5 simulated illumination (Newport, 91192) with a power density of 100 mW cm^{-2}. Electrochemical impedance spectroscopy (EIS) measurements were also performed on CHI 660C with the frequency ranging from 100 kHz to 0.1 Hz under the bias voltage of 0.7 V in the illumination.

3. Results and discussion

3.1. Characterization of the carbon/SnO_2/TiO_2 counter electrode

Fig. 1 showed XRD patterns of the carbon/SnO_2/TiO_2 composite film with 30% SnO_2 content. The peaks at about $2\theta = 26.6°$ and 54.7° corresponded to (0 0 2) and (0 0 4) planes of the graphite, respectively. Graphite in carbon black was supposed to offer a good electrical conductivity for the counter electrode. The peak at $2\theta = 25.5°$ corresponded to (1 0 1) plane of TiO_2, which described anatase crystallite. Other peaks at $2\theta = 26.7°$, 33.9° and 51.8° in the XRD patterns were attributed to (1 1 0), (1 0 1) and (2 1 1) planes of SnO_2, respectively (The Joint Committee on Powder Diffraction Standards, No: 44-1294). The morphologies of as-prepared carbon/SnO_2/TiO_2 composite film were obtained by scanning electron microscopy

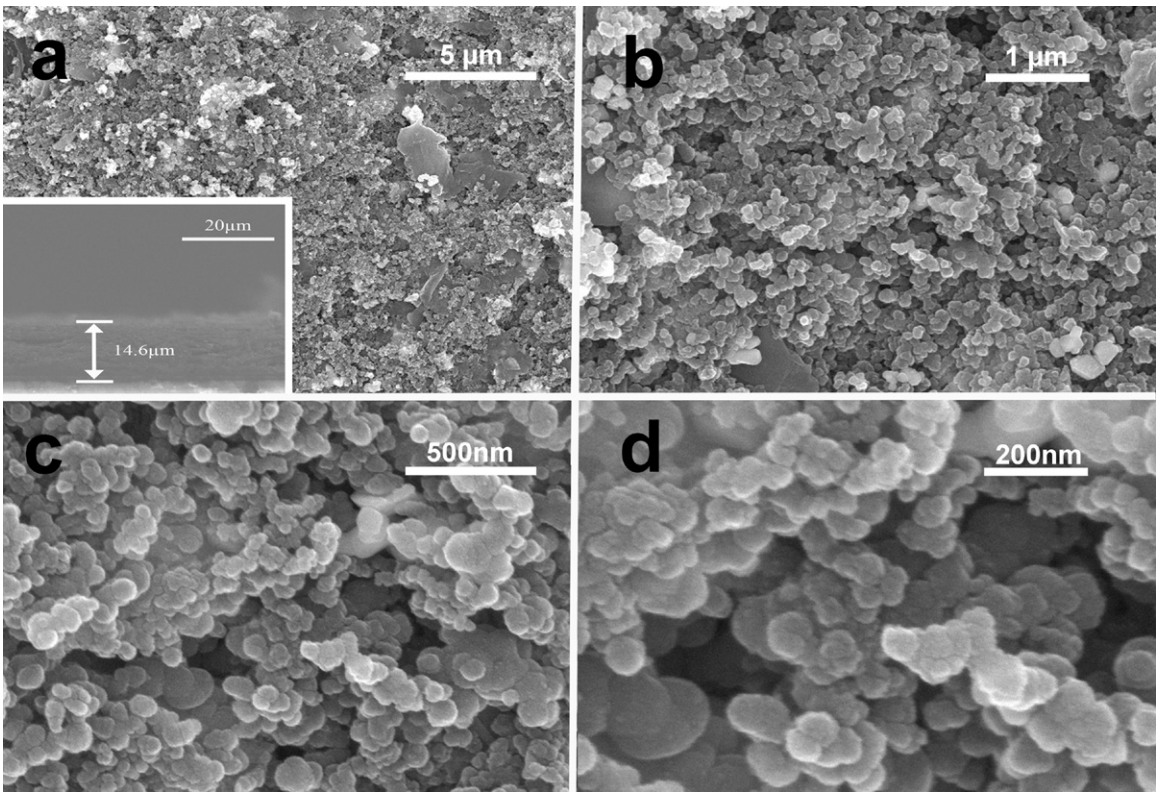

Fig. 2. Top view SEM images of (a–d): the carbon/SnO_2/TiO_2 composite layer with different magnification. Inset of (a) shows cross-section SEM image of the carbon/SnO_2/TiO_2 composite layer. The SnO_2 content is 30%.

(SEM). Fig. 2a–d showed the morphology of the nanocomposite under different magnifications. It was clear that as-prepared carbon/SnO_2/TiO_2 composite film had a highly porous structure and there was good contact among individual nanoparticles. This mesoporous structure made I_3^- ions with a size of only a few angstroms diffused throughout the composite film favorably and thus the entire surface area would available for I_3^- reduction [18,19]. Consequently, such character made the mesoporous nanocomposite counter electrode possess a large surface area and a better catalytic activity than Pt counter electrode, which was well proved by cyclic voltammetry. A cross-section SEM view (Fig. 2a, inset) indicated that the average thickness of the carbon film was about 14.6 μm.

The as-prepared carbon/SnO_2/TiO_2 composite film was further characterized by transmission electron microscopy (TEM), as shown in Fig. 3. Fig. 3a showed typical TEM images for the composite film. The metallic oxides were well mixed with carbon and the interconnected 3D network structures were confirmed. A selected area high-resolution TEM (HR-TEM) image of carbon/SnO_2/TiO_2 composite was shown in Fig. 3b. The width of 0.33 nm between neighboring fringes of SnO_2 nanoparticles corresponded to the (1 1 0) planes (Fig. 3b). Energy-dispersive X-ray analysis (EDX) results confirmed the presence of all C, Sn, Ti and O in carbon/SnO_2/TiO_2 composite film (Fig. 3a, inset).

3.2. Influence of SnO_2 content on the performance of DSSCs

The carbon counter electrodes with various SnO_2 content were also studied. As shown in Fig. 4a, short-circuit current (J_{sc}), fill factor (FF) and the power conversion efficiency (PCE) of DSSCs increased with the addition of SnO_2 power and reached a peak value at SnO_2 content of 30%, and then decreased with further increasing of the SnO_2 content. To investigate the reason of the difference in DSSCs performance with various SnO_2 content, the BET surface areas and root-mean-square roughness (R_{rms}) of each film were measured (see Fig. 4b). The BET surface areas and R_{rms} increased with increasing of SnO_2 content at first and decreased later on. When the SnO_2 content was 30%, the highest BET surface areas and R_{rms} were obtained to be 221 $m^2\ g^{-1}$ and 928 nm, respectively. Simultaneously, the cell achieved the highest efficiency of 6.15% at this concentration. It suggested that the increasing BET surface area and root-mean-square roughness of the film improved the short-circuit current and efficiency of DSSCs. In fact, it was observed that the carbon film with SnO_2 added showed a good mechanical stability while the film without SnO_2 could crack easily during the test. This was mainly because SnO_2 could also act as network to well cement carbon film, which in turn increased the fill factor. However, a much more SnO_2 content would decrease the electrical conductivity as well as the fill factor of the carbon film.

3.3. Cyclic voltammetry for the optimum carbon/SnO_2/TiO_2 counter electrode

The catalytic activity of the optimum carbon/SnO_2/TiO_2 counter electrode and Pt counter electrode toward I^-/I_3^- redox couple were compared by cyclic voltammetry under the same condition (see Fig. 5). There were two pairs of oxidation/reduction peaks for both electrodes, which indicated that they all have catalytic activity to I^-/I_3^- redox couple [19]. Though the exact charge-transfer mechanisms were not fully understood, literatures attributed two pairs of peaks to two equations. The left pairs were assigned to the oxidation Eq. (1) and the right pairs were assigned to the reduction Eq. (2), respectively [8,20].

$$I_3^- + 2e^- \rightleftarrows 3I^- \quad (1)$$

$$3I_2 + 2e^- \rightleftarrows 2I_3^- \quad (2)$$

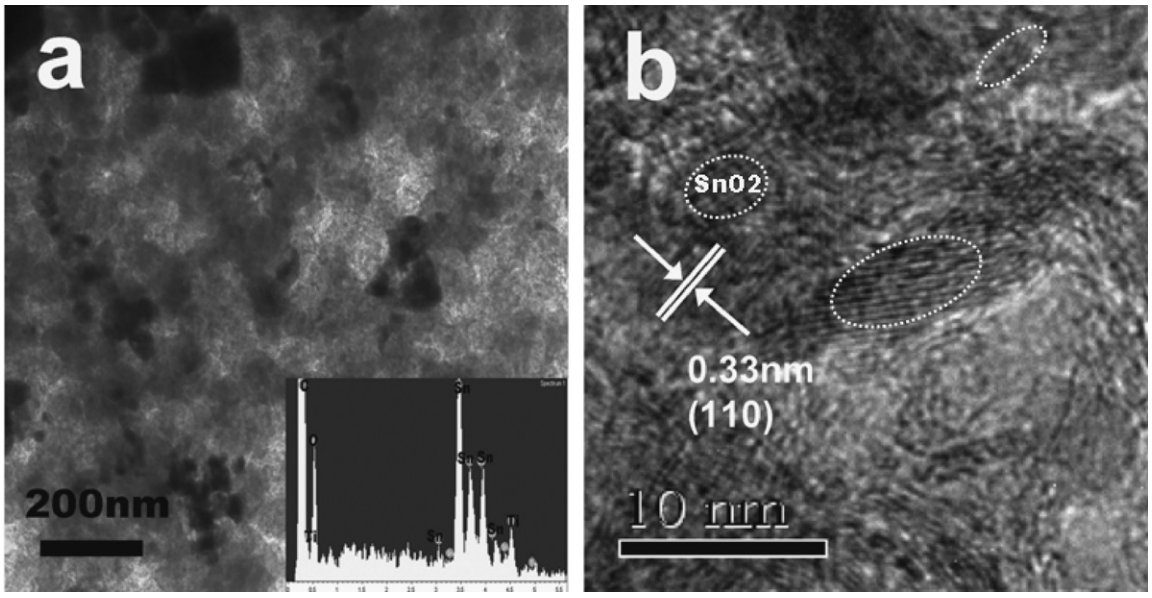

Fig. 3. (a) TEM image of the carbon/SnO_2/TiO_2 nanocomposite revealing the interconnected 3D porous structure. (b) Selected area HR-TEM image of the carbon/SnO_2/TiO_2 nanocomposite showing the presence of SnO_2. Inset of (a) shows EDX pattern of the carbon/SnO_2/TiO_2 nanocomposite. The SnO_2 content is 30%.

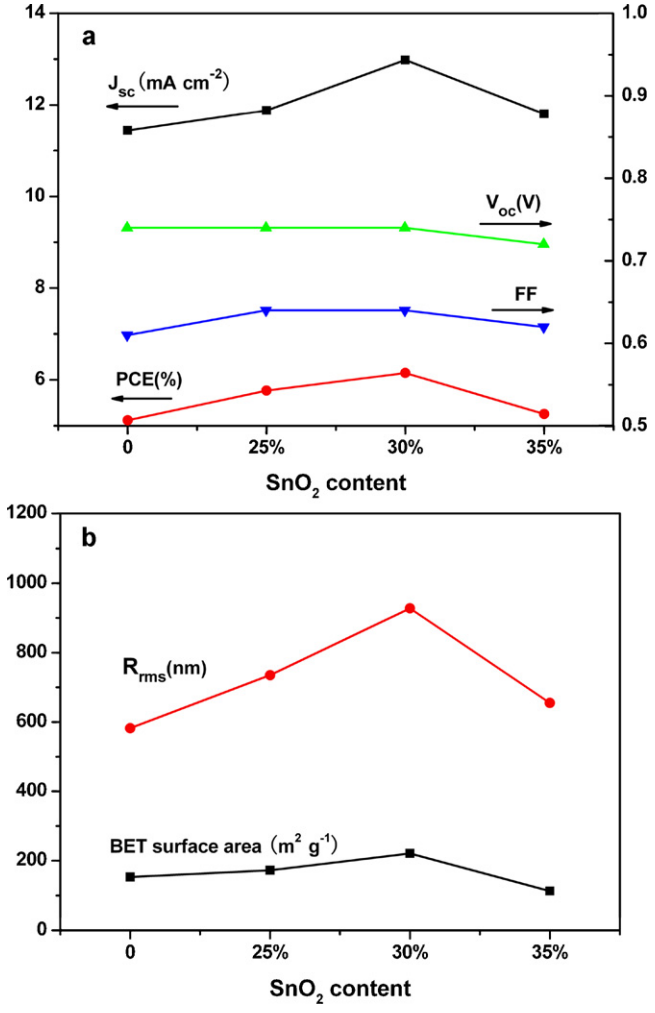

Fig. 4. (a) The relation between photovoltaic parameters and the SnO_2 content in the nanocomposite counter electrode. (b) R_{rms} and BET Surface Areas of the nanocomposite counter electrode with various SnO_2 content. The SnO_2 content is the weight ratio of SnO_2 and carbon powder.

As known to us, the counter electrode in DSSCs served as catalyst to reduce I_3^- to I^- in the electrolyte, thus the characteristics of the left pair of peaks were of interest. The peak current density could be used to evaluate the catalytic activity of the counter electrodes [21,22]. From Fig. 5, we could see that carbon/SnO_2/TiO_2 counter electrode exhibited higher catalytic ability even than Pt counter electrode for its higher peak current density. This result suggested that the composite counter electrode had a large inner electrode surface area for I_3^- ions reduction and hence the carbon/SnO_2/TiO_2 composite could be used as an efficient counter electrode in DSSCs.

3.4. Electrochemical impedance spectroscopy analysis

Electrochemical impedance spectroscopy (EIS) analysis was regarded as a useful tool for investigating the charge transport on the counter electrode in DSSCs. To further characterize the catalytic properties of the optimum carbon/SnO_2/TiO_2 counter electrode, the electrochemical impedance spectroscopy of DSSCs based on

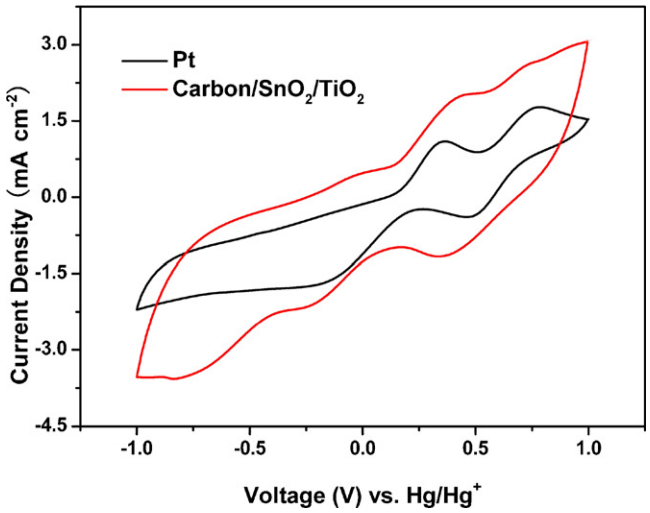

Fig. 5. Cyclic voltammetry of Pt and the carbon/SnO_2/TiO_2 counter electrode at a scan rate of 50 mV s^{-1} in 10 mM LiI, 1 mM I_2 and 0.1 M $LiClO_4$ in acetonitrile solution. Reference electrode: Hg/Hg^+ reference electrode in acetonitrile.

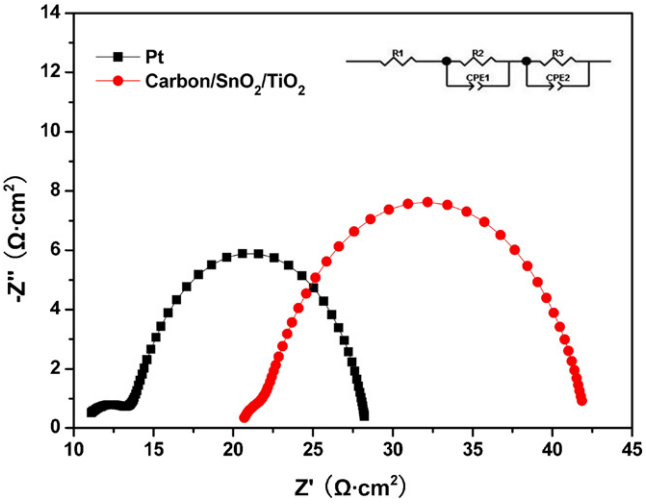

Fig. 6. Electrochemical impedance spectroscopy of the cells based on sputtering Pt and the carbon/SnO_2/TiO_2 counter electrode obtained at open circuit conditions under one sun illumination (AM 1.5–100 mW cm^{-2} simulated irradiation) with active area of 0.25 cm^2, according to the inset equivalent circuit model. R_1: serial resistance, R_2: the electron transfer and recombination in TiO_2/dye/electrolyte interfaces, R_3: charge-transfer resistance of counter electrode; CPE1: constant phase element of TiO_2/dye/electrolyte interfaces, CPE2: constant phase element of the FTO/TiO_2 and counter electrode/electrolyte interfaces. The impendence of CPE is described as $Z_{CPE} = Q(j\omega)^{-n}$ ($0 \le n \le 1$). Q and n are frequency-independent parameters of the CPE.

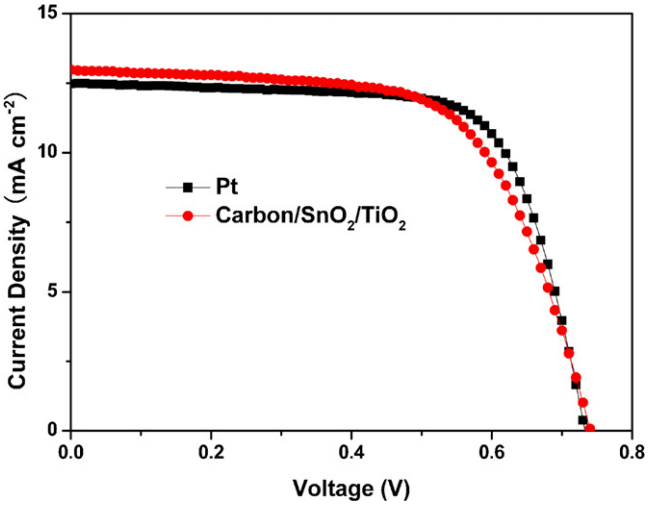

Fig. 7. Photocurrent–voltage characteristics of DSSCs employing sputtering Pt and the carbon/SnO_2/TiO_2 counter electrode measured under one sun illumination (AM 1.5–100 mW cm^{-2} simulated irradiation) with active area of 0.25 cm^2.

Pt–CE and the carbon/SnO_2/TiO_2–CE was measured in the illumination at open circuit conditions. Fig. 6 showed Nyquist plots of Pt- and the carbon/SnO_2/TiO_2-based DSSCs. The Nypuist diagram of DSSCs observed in the frequency regions of 10^3–10^5 Hz, 1–10^3 Hz and 0.1–1 Hz were associated with the charge transfer impedance (R_3) at the FTO/TiO_2 and counter electrode/electrolyte interfaces, the electron transfer and recombination in TiO_2/dye/electrolyte interfaces (R_2), and the Nernst diffusion in the electrolyte, respectively [23–25]. Since an identical photoanode was employed in DSSCs, the difference at the counter electrode/electrolyte interfaces was wholly responsible for the variation of R_3. By fitting the experimental data with the inset equivalent circuit containing a constant phase element (CPE) and resistance (R), charge transfer resistance (R_3) at the counter electrode/electrolyte interfaces and device's series resistance (R_1) could be obtained (see Table 1) [26]. R_1 of DSSCs based on the carbon/SnO_2/TiO_2 counter electrode (20.11 Ω cm^2) was higher than that of Pt (14.32 Ω cm^2), which probably caused by the carbon/SnO_2/TiO_2 composite counter electrode had much higher resistivity than that of platinum [13]. It could affect the fill factor of the device [27]. However, the R_3 value of the carbon counter electrode was 1.64 Ω cm^2, which was observed less than half of that in Pt counter electrode (3.58 Ω cm^2). Even though apparent reaction rate per unit area of carbon is less than that of platinum, the lower charge transfer resistance of the carbon/SnO_2/TiO_2 counter electrode benefited from its mesoporous nature and large inner electrode surface area according to the results of SEM and BET. This feature counterbalanced the higher series resistance of the cell and helped to achieve overall conversion efficiency comparable to that of Pt based device.

Table 1
EIS and J–V Parameters of DSSCs with Pt and Carbon/SnO_2/TiO_2 nanocomposite counter electrode.

Electrodes	R_1 (Ω cm^2)	R_3 (Ω cm^2)	V_{oc} (V)	J_{sc} (mA cm^{-2})	FF	PCE (%)
Pt	14.32	3.58	0.73	12.47	0.71	6.48
Carbon	20.11	1.64	0.74	12.98	0.64	6.15

3.5. Photovoltaic performance of DSSCs based on the carbon counter electrode

Fig. 7 showed photocurrent–voltage characteristics of DSSCs employing Pt and the optimum carbon/SnO_2/TiO_2 counter electrodes under AM 1.5, 100 mW cm^{-2} illumination with active area of 0.25 cm^2. The DSSCs based on the carbon/SnO_2/TiO_2 counter electrodes exhibited a short current density (J_{sc}) of 12.98 mA cm^{-2}, an open circuit voltage (V_{oc}) of 0.74 V, and a fill factor (FF) of 0.64, corresponding to a power conversion efficiency (PCE) of 6.15%, which was nearly 95% compared to PCE of Pt-based devices (6.48%) at the same condition (see Table 1). Compared with the Pt-based DSSCs, the most pronounced change by using nano-composite counter electrode was the increase of J_{sc} and V_{oc} with compensation of FF decrease. The FF of the carbon/SnO_2/TiO_2 composite based DSSCs was lower than Pt based DSSCs, which was ascribed to the higher series resistance of the composite electrode as EIS had studied. And the large surface areas, high root-mean-square roughness and its mesoporous nature of the carbon/SnO_2/TiO_2 counter electrode were responsible for the increase of J_{sc}.

4. Conclusion

In conclusion, we have prepared a low cost mesoporous carbon/SnO_2/TiO_2 nanocomposite counter electrode using SnO_2 as "framework". The BET surface areas and root-mean-square roughness of the carbon film were significantly improved with increasing the SnO_2 concentration to 30%, which enhanced the short-circuit current, FF and the efficiency at the same time. The optimum counter electrode revealed higher catalytic activity and lower R_{ct} compared with Pt counter electrode. Finally, dye-sensitized solar cells employing this counter electrode achieve efficiency as high as 6.15% which was comparable to that of the cells using sputtering Pt as counter electrode (6.48%) at similar conditions. The carbon/SnO_2/TiO_2 composite counter electrode demonstrated much lower cost and almost the same power conversion efficiency compared with Pt electrode, which made it suitable in DSSCs commercial applications.

Acknowledgements

The authors gratefully thank for the financial support of this work by the National Basic Research Program of China (grant no.

2011CB933300) and the National Science Fund for Talent Training in Basic Science (grant no. J0830310).

References

[1] B. O'Regan, M. Grätzel, Nature 353 (1991) 737.
[2] M. Grätzel, Nature 414 (2001) 338.
[3] M.K. Nazeeruddin, A. Kay, I. Rodicio, R. Humphry-Baker, E. Müller, P. Liska, N. Vlachopoulos, M. Grätzel, J. Am. Chem. Soc. 115 (1993) 6382.
[4] B. O'Regan, D.T. Schwartz, S.M. Zakeeruddin, M. Grätzel, Adv. Mater. 12 (2000) 1263.
[5] X. Fang, T. Ma, G. Guan, M. Akiyama, E. Abe, J. Photochem. Photobiol. A 164 (2004) 179.
[6] N. Papageorgiou, W. Maier, M. Grätzel, J. Electrochem. Soc. 144 (1997) 876.
[7] A. Kay, M. Grätzel, Sol. Energy Mater. Sol. Cells 44 (1996) 99.
[8] Z. Huang, X. Liu, K. Li, D. Li, Y. Luo, H. Li, W. Song, L.Q. Chen, Q. Meng, Electrochem. Commun. 9 (2007) 596.
[9] K. Li, Y. Luo, Z. Yu, M. Deng, D. Li, Q. Meng, Electrochem. Commun. 11 (2009) 1346.
[10] S.I. Cha, B. Koo, S. Seo, D.Y. Lee, J. Mater. Chem. 20 (2009) 659.
[11] W.J. Lee, E. Ramasamy, D.Y. Lee, J.S. Song, Sol. Energy Mater. Sol. Cells 92 (2008) 814.
[12] T.N. Murakami, S. Ito, Q. Wang, M.K. Nazeeruddin, T. Bessho, I. Cesar, P. Liska, R. Humphry-Baker, P. Comte, P. Pechy, J. Electrochem. Soc. 153 (2006) A2255.
[13] P. Joshi, Y. Xie, M. Ropp, D. Galipeau, S. Bailey, Q. Qiao, Energy Environ. Sci. 2 (2009) 426.
[14] Y. Liu, J. Xie, Y. Takeda, J. Yang, J. Appl. Electrochem. 32 (2002) 687.
[15] M.Y. Li, C.L. Liu, Y. Wang, W.S. Dong, J. Electrochem. Soc. 158 (2011) 296.
[16] R.L. Willis, C. Olson, B. O'Regan, T. Lutz, J. Nelson, J.R. Durrant, J. Phys. Chem. B 106 (2002) 7605.
[17] J.J. Niu, J.N. Wang, N.S. Xu, Solid State Sci. 10 (2008) 618.
[18] E. Ramasamy, W.J. Lee, D.Y. Lee, J.S. Song, Appl. Phys. Lett. 90 (2007) 173103.
[19] S. Peng, F. Cheng, J. Shi, J. Liang, Z. Tao, J. Chen, Solid State Sci. 11 (2009) 2051.
[20] P. Li, J. Wu, J. Lin, M. Huang, Y. Huang, Q. Li, Sol. Energy 83 (2009) 845.
[21] J.D. Roy-Mayhew, D.J. Bozym, C. Punckt, I.A. Aksay, ACS Nano (2010).
[22] H. Sun, Y. Luo, Y. Zhang, D. Li, Z. Yu, K. Li, Q. Meng, J. Phys. Chem. C (2010).
[23] S. Gagliardi, L. Giorgi, R. Giorgi, N. Lisi, T. Dikonimos Makris, E. Salernitano, A. Rufoloni, Superlatt. Microstruc. 46 (2009) 205.
[24] M. Adachi, M. Sakamoto, J. Jiu, Y. Ogata, S. Isoda, J. Phys. Chem. B 110 (2006) 13872.
[25] J. Bisquert, J. Phys. Chem. B 106 (2002) 325.
[26] Q.D. Tai, B.L. Chen, F. Guo, S. Xu, H. Hu, B. Sebo, X.Z. Zhao, Acs Nano 5 (2011) 3795.
[27] F. Fabregat-Santiago, J. Bisquert, E. Palomares, L. Otero, D. Kuang, S.M. Zakeeruddin, M. Grätzel, J. Phys. Chem. C 111 (2007) 6550.